Atomistic models of the Si(100)–SiO_2 interface: structural, electronic and dielectric properties

2005 J. Phys.: Condens. Matter 17 S2065

(http://iopscience.iop.org/0953-8984/17/21/003)

INSTITUTE OF PHYSICS PUBLISHING JOURNAL OF PHYSICS: CONDENSED MATTER

J. Phys.: Condens. Matter **17** (2005) S2065–S2074 doi:10.1088/0953-8984/17/21/003

Atomistic models of the Si(100)–SiO_2 interface: structural, electronic and dielectric properties

Feliciano Giustino[1], **Angelo Bongiorno**[2] **and Alfredo Pasquarello**

Ecole Polytechnique Fédérale de Lausanne (EPFL), Institute of Theoretical Physics, CH-1015 Lausanne, Switzerland
and
Institut Romand de Recherche Numérique en Physique des Matériaux (IRRMA), CH-1015 Lausanne, Switzerland

E-mail: feliciano.giustino@epfl.ch

Received 10 December 2004
Published 13 May 2005
Online at stacks.iop.org/JPhysCM/17/S2065

Abstract

We review the structural, electronic and dielectric properties of atomistic models of the Si(100)–SiO_2 interface, which have been purposely designed in order to match a large variety of atomic-scale experimental data. After describing the generation procedure and the structural properties of two specific interface models, we study the corresponding electronic structure and dielectric response within the framework of density-functional theory. Particular emphasis is given to a systematic comparison between the atomistic properties of our model interfaces and experiment. Besides synthesizing the present status of our experimental knowledge on the Si(100)–SiO_2 interface, these models provide a solid and necessary basis for future investigations in the area of gate stacks for Si-based microelectronics.

1. Introduction

The need for increasing circuit density while keeping unchanged the power consumption in integrated metal–oxide–semiconductor devices translates into the requirement of larger gate capacitance for each new technology generation. To date, the increase of the gate capacitance has mainly been achieved by reducing the thickness of the gate oxide [1], reaching values as small as 2 nm [2]. As a consequence, the interfacial transition layer between silicon and its oxide has become a significant fraction of the total thickness and its detailed physical properties have a strong impact on device performance [2]. Despite the major effort which is nowadays devoted to the replacement of SiO_2 by materials of higher dielectric permittivity [3],

[1] Author to whom any correspondence should be addressed.
[2] Present address: School of Physics, Georgia Institute of Technology, Atlanta, GA 30332-0430, USA.

the transition layer between Si and SiO_2 still plays a central role. Indeed, during the post-deposition annealing for dopant activation, oxygen atoms diffuse out of the transition metal silicate and oxidize the Si substrate, forming an interfacial oxide layer [4]. Understanding the structural, electronic and dielectric properties of this interfacial layer is therefore of paramount importance for the progress of Si-based microelectronics.

Several experimental techniques [5] have provided detailed atomic-scale information on the bonding pattern at the Si(100)–SiO_2 interface. The amorphous nature of the oxide is clearly indicated by both transmission electron microscopy and x-ray scattering [5]. The density of the oxide near to the substrate is higher than that of vitreous silica by at most 10% [6, 7]. Electrical characterization [8] and electron spin resonance measurements [9] reveal extremely low densities of interface states. Additional information on the atomistic structure of the interfacial region comes from photoemission spectroscopy, which reveals the occurrence of three intermediate oxidation states of Si [10–13], corresponding to Si atoms with different O coordinations [14, 15, 19]. The dielectric properties of the interfacial layer have been probed less extensively. Auger spectroscopy measurements suggest that, at a distance of 6 Å from the substrate, the oxide permittivity has already recovered the bulk SiO_2 value [20]. Furthermore, from electrical measurements on SiO_2/ZrO_2 capacitors with varying ZrO_2 thickness, a permittivity between 6 and 7 has tentatively been assigned to the interfacial oxide [21].

Several structural models of the Si(100)–SiO_2 interface have recently been proposed [14–18, 22–30]. However, none of these models matches the full list of atomic-scale properties mentioned above. The generation of a *realistic* model of the Si(100)–SiO_2 interface is nevertheless a goal of primary importance. From a fundamental point of view, this would demonstrate that the information resulting from various experimental probes can indeed be assembled consistently in well defined atomistic structures. Furthermore, on the practical side, the realization of such a model would synthesize the present status of our experimental knowledge on the Si(100)–SiO_2 interface, providing the necessary basis for future investigations in the area of high-permittivity gate stacks, which often incorporate a SiO_2 interlayer.

The purpose of the present work is to review the structural, electronic and dielectric properties of two atomistic models of the Si(100)–SiO_2 interface, which have been generated with the specific intent of incorporating the available atomic-scale experimental data. After describing the generation procedure in section 2, we present the corresponding structural properties in section 3. The electronic and dielectric properties of these model interfaces are analysed in sections 4 and 5, respectively.

2. Generation of models with disordered oxides

Our target consisted in generating model interfaces with the following atomic-scale properties derived from experiment. First, our model structure should reproduce the disordered nature of the oxide [5]. Second, our model structure should be consistent with the extremely low density of coordination defects (one defect out of 300 Si interface atoms) [8, 9]. Third, the mass density profile in our model structure should agree with x-ray reflectivity measurements, which yield an oxide density in proximity to the Si substrate between 2.3 and 2.4 g cm^{-3} [6, 7], slightly denser than vitreous silica (2.2 g cm^{-3}). Fourth, the transition region in our model structure should contain Si atoms in intermediate oxidation states in accord with Si 2p core-level photoemission experiments [12, 13]. Following the commonly accepted interpretation scheme [10, 11, 14, 15, 19], recent photoemission experiments yield 1.8 monolayers (1 ML $= 6.5 \times 10^{14}$ atoms cm^{-2}) of partially oxidized Si atoms, distributed

between Si^{1+}, Si^{2+}, and Si^{3+} moieties according to the ratio of 1:2:3 [12, 13]. From recent angle-resolved spectra obtained with synchrotron radiation [12, 13], one deduces in addition that the Si^{1+} and Si^{2+} moieties are located right at the interface, while the Si^{3+} ones are distributed within a few Si–O bond lengths from the interface.

To generate model structures of the Si(100)–SiO_2 interface, we used a two-step procedure [31]. In the first step, we constructed a suitable topological connection between the substrate and the oxide. For this purpose, we used classical molecular dynamics [32] at 3500 K to evolve Si and O atoms in the presence of a template of fixed Si atoms representing the substrate. A slow quench (10 K ps^{-1}) to low temperatures provided us with oxides attached to the template without any coordination defect. By varying the positions of the Si atoms in the template, we obtained model structures showing different bonding patterns at the interface. During the molecular dynamics simulation, the mass density of the oxide was controlled by setting from the outset the size of the simulation cell. The template exposes two (100) opposite faces to the oxide within an orthorhombic supercell. From a single oxide/template/oxide superstructure, we constructed two model interfaces by 'cutting' the system halfway through the template and halfway through the oxide. Then, the template in both models was extended by adding Si(100) monolayers. The unsaturated bonds at the outer surfaces were terminated with H atoms. The final model structures of the Si(100)–SiO_2 interface are periodic in directions parallel to the interface with a $\sqrt{8} \times \sqrt{8}$ repeat unit of interface Si atoms. For a repeat unit of this size, the low experimental density of interface defects [9] is best described by a perfect bonding network, as is the case for the present model structures.

In the second step, the model structures were further optimized. First, the targeted distribution of partially oxidized Si atoms was achieved by removing a few O atoms from the oxide. This extended the range of partially oxidized Si atoms into the oxide region. Second, we recovered optimal structural parameters by performing a complete structural relaxation within a density-functional scheme (*vide infra*).

Among the models generated in this way, we made a further selection by performing ion-scattering simulations and comparing the results for each interface model with experiment [33]. In the channelling geometry, ion-scattering experiments measure the number of 'excess Si atoms' at the Si(100)–SiO_2 interface [34]. The excess Si yield is a genuine interface property which includes Si atoms in intermediate oxidation states as well as a measure of the in-plane Si displacements at the interface [34]. To extract atomic scale information, we addressed a set of atomistic interface models with bond patterns of varying complexity [31]. Measured and calculated ion-scattering yields were initially compared for ion energies ranging between 0.4 and 1.0 MeV [33]. The comparison was then extended to ion energies up to 2.0 MeV [35]. The ion-scattering analysis showed that

(i) Si atoms in intermediate oxidation states contribute to the excess Si yield by approximately 0.8 ML,
(ii) silicon in-plane distortions larger than 0.09 Å propagate from the interface into the three upper layers of the Si lattice, and
(iii) these distortions are consistent with transition structures showing a significant degree of disorder in the bonding pattern.

Among the many generated models, we retained only two of them showing excess Si yields closest to the experimental result. These two models will hereafter be referred to as to model I and model II[3]. In model I, the terminating Si layer shows a high density of in-plane Si–Si dimers, with a high fraction of oxidized backbonds. In model II, the structure of the terminating Si layer

[3] Model I and model II correspond to model B and model C′ of [33], respectively.

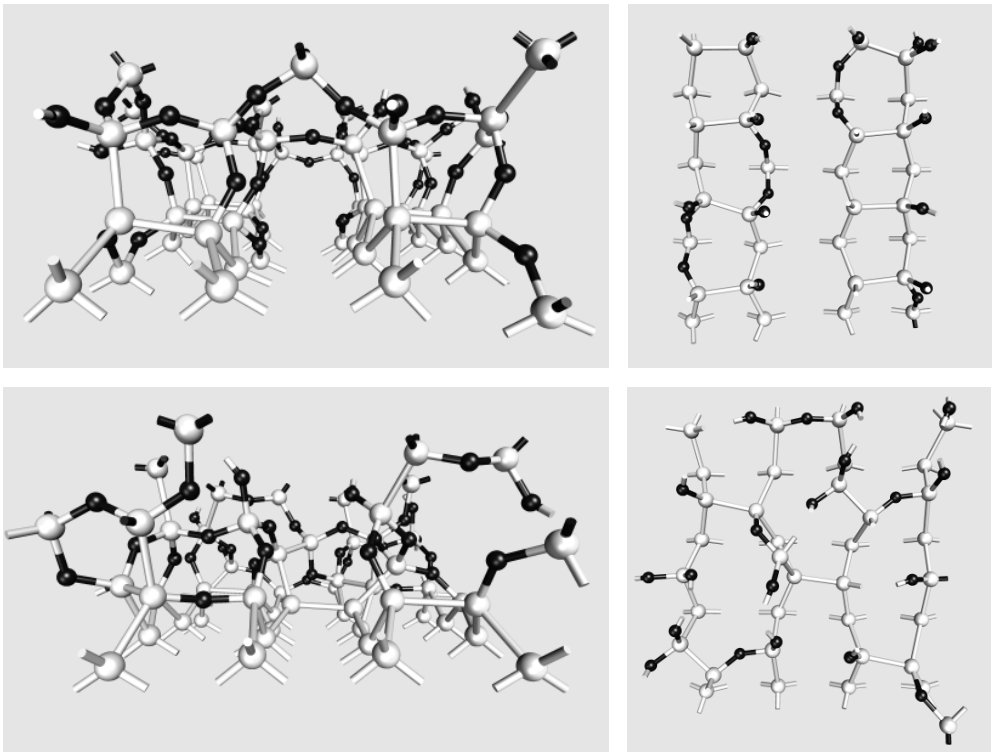

Figure 1. Ball-and-stick representation of the transition layer in the model structures of the Si(100)–SiO_2 interface considered in this work: side and top views of model I (top panels) and model II (bottom panels). Grey balls indicate Si atoms, black balls O atoms.

is adapted from a model generated previously by first-principles molecular dynamics [22, 23]. A ball-and-stick representation of these models is given in figure 1.

For the specific purpose of studying the electronic and dielectric properties of these models, we found it convenient to dispose of the silicon/vacuum and oxide/vacuum interfaces occurring in the original models by adopting superlattice geometries. Hence, we mirrored each model interface with respect to the interface plane, so as to obtain two opposite Si–SiO_2 and SiO_2–Si junctions, separated by empty space. Subsequently, we generated stoichiometric SiO_2 in the region between the junctions by means of classical molecular dynamics. The size of the simulation cell in the direction orthogonal to the interface planes was fixed so as to obtain melts at the experimental density of vitreous SiO_2. The superlattice arrangements were then obtained through the matching of the Si lattices. In order to release the residual strain, we again relaxed the atomic positions in the model structures through first-principle molecular dynamics (*vide infra*). The final structures consisted of 315 and 313 atoms, respectively, distributed in 13 Si layers and 2.5 nm of oxide, within simulation cells of size $\simeq 11 \times 11 \times 45$ Å^3.

In our first-principles scheme, the electronic structure was described by using a plane-wave basis set for the valence wavefunctions and pseudopotentials to account for the core–valence interactions. We used a norm-conserving pseudopotential for Si atoms [36] and an ultrasoft pseudopotential for O atoms [37]. The exchange and correlation energy was accounted for within the generalized gradient approximation of Perdew and Wang [38]. We carried out structural relaxations adopting a damped molecular-dynamics scheme [39–41]. Energy cut-

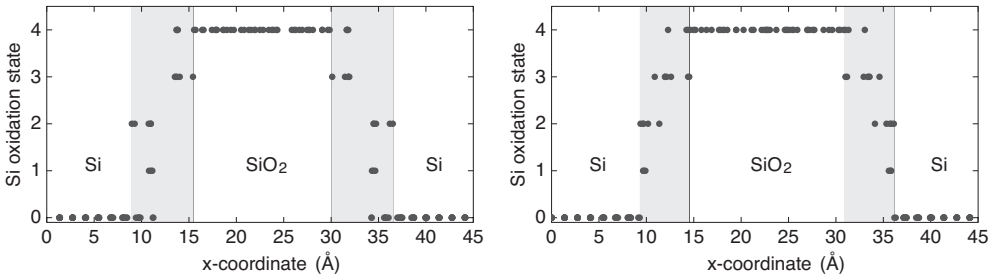

Figure 2. Distribution of Si atoms in model I (left) and model II (right) of the Si(100)–SiO_2 interface according to the corresponding oxidation state (vertical scale). The shaded areas indicate the suboxide regions, and the x-coordinate is along a direction perpendicular to the interface plane. The models are shown in the periodic superlattice arrangement.

Table 1. Average Si–O bond length, Si–O–Si and O–Si–O bond angles for model I and model II of the Si(100)–SiO_2 interface. The standard deviations of the corresponding distributions are given between brackets. We report separately the values for the suboxide regions and for the stoichiometric oxide. Experimental data refer to bulk vitreous silica.

	Model I		Model II		Experiment
	Suboxide	Si^{4+}	Suboxide	Si^{4+}	Si^{4+}
Si–O (Å)	1.65(0.02)	1.64(0.02)	1.67(0.03)	1.64(0.02)	1.61
∠Si–O–Si	140.9° (6.1)	143.0° (13.2)	130.7° (9.3)	144.3° (14.1)	147°–151°[a]
∠O–Si–O	106.4° (5.9)	109.5° (6.8)	107.6° (7.3)	109.4° (6.3)	109.4°

[a] Reference [43].

offs of 24 and 150 Ryd were used for the wavefunctions and for the augmented electron density, respectively.

3. Structural properties

Average structural parameters for bond lengths and bond angles of model I and model II of the Si(100)–SiO_2 interface are given in table 1. Si–O bond lengths associated with partially oxidized Si atoms are generally longer than the mean bond length in SiO_2, due to the less electronegative suboxide environment [42]. Bond angle distributions do not show any particular dependence on Si oxidation state or on distance from the interface. The tetrahedral coordination of the Si atoms is well preserved, both in the oxide and in the suboxide region (table 1). The mean Si–O–Si bond angle is close to that of vitreous silica [43].

The model structures contain the same distribution of partially oxidized Si atoms, in accord with recent photoemission data [12, 13]. More specifically, our model structures contain 0.3, 0.7 and 0.9 ML of Si^{1+}, Si^{2+} and Si^{3+} moieties, respectively. The Si^{1+} and Si^{2+} are located right at the interface while the Si^{3+} moieties are distributed in the oxide within a range of three to four Si–O bond lengths from the interface (figure 2). Overall, the suboxide region (i.e. the region containing the partially oxidized Si atoms) was found to be 6.4 and 5.1 Å thick for interface models I and II, respectively.

The mass density was evaluated for layers of increasing thickness starting at the interface and extending into the oxide. The average mass density was found to decay slowly from about 2.3 g cm^{-3} in the immediate vicinity of the interface to 2.2 g cm^{-3} and 2.1 g cm^{-3} deep into the stoichiometric oxide of interface models I and II, respectively. These results are in agreement

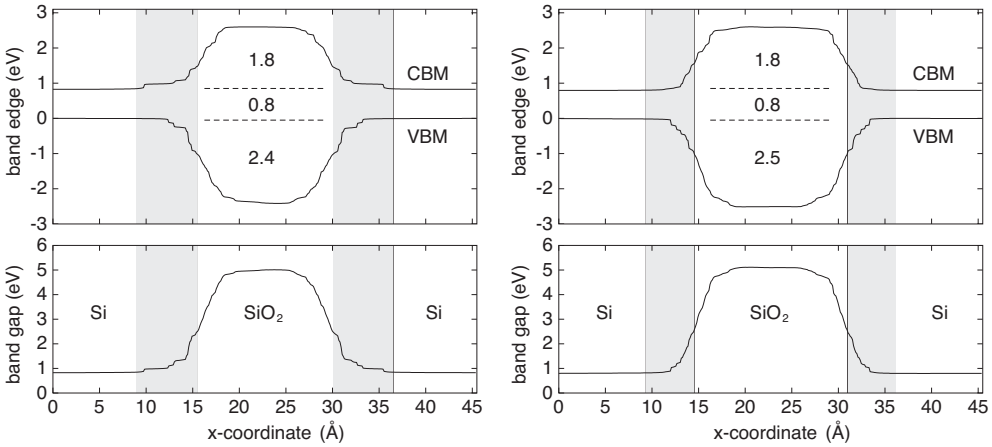

Figure 3. Conduction band minimum (CBM), valence band maximum (VBM) and bandgap profiles across model I (left) and model II (right) of the Si(100)–SiO_2 interface. The shaded areas indicate the suboxide regions. The x-coordinate is along a direction perpendicular to the interface plane. The models were recast into a periodic geometry in order to eliminate surface dipoles arising from asymmetric terminations.

with x-ray reflectivity experiments which indicate the occurrence of a thin interfacial oxide layer of mass density ranging between 2.3 and 2.4 g cm^{-3} [6, 7].

Simulations with ion energies between 0.4 and 1.0 MeV gave excess Si yields of 2.7 and 2.9 ML for model I and model II, respectively. These values compare well with the experimental result of 3.0 ± 0.3 ML [33]. In addition, model II was found to match the ion-scattering data for ion energies ranging up to 2 MeV [35] and to reproduce the experimental strain versus depth profile [44] associated with distortions in the direction perpendicular to the plane of the interface [45].

4. Electronic properties

The valence band maximum (VBM) and the conduction band minimum (CBM) of our model interfaces were determined as follows. First, we calculated the local density of states according to

$$D(x;\epsilon) = 2\sum_n |\langle x|\psi_n\rangle|^2 \delta(\epsilon - \epsilon_n), \tag{1}$$

where x indicates a coordinate along the interface normal, $|\psi_n\rangle$ are the eigenstates of the Kohn–Sham Hamiltonian with eigenvalues ϵ_n, and the sum extends over both occupied and empty states. The Dirac delta functions in equation (1) were conveniently replaced by Gaussian functions with a standard deviation of 0.01 eV. Then, for every value of x, we determined the local band edges by requiring that the number of states falling between the supercell midgap and the band-edge equals a threshold value of 0.1 states/$Å^3$ [26]. To determine the bulk band edges deep inside the Si and SiO_2 layers we adopted the double macroscopic average according to [46].

In figure 3, we report the local CBM, the VBM and the local bandgap for both model interfaces. The main features are also summarized in table 2. Deep inside the Si layer, we found a bandgap of 0.8 eV for both interface models. The gap in the oxide amounts to 5.0 and 5.1 eV for model I and model II, respectively. The 0.1 eV difference arises from the slightly

Table 2. Calculated bandgaps and band offsets (in units of eV) for models I and II of the Si(100)–SiO_2 interface.

	E_{gap}^{Si}	$E_{gap}^{SiO_2}$	ΔE_v	ΔE_c
Model I	0.8	5.0	2.4	1.8
Model II	0.8	5.1	2.5	1.8
Experiment	1.1	8.9	4.3[a]	3.0[b]

[a] Reference [47].
[b] Reference [48], assuming a Si bandgap of 1.1 eV.

different mass densities in the middle of the oxide region. The corresponding experimental values (1.1 and 8.9 eV for Si and SiO_2, respectively) are underestimated by about a factor of two, as usual in density-functional calculations. The calculated valence band offsets are 2.4 eV for model I and 2.5 eV for model II, while the corresponding conduction band offsets are 1.8 eV for both interface models. As for the bandgaps, the calculated band offsets underestimate the experimental values of 3.1 and 4.3 eV [47, 48]. However, the calculated values agree with other calculations for more idealized models of the Si(100)–SiO_2 interface [26, 49, 50]. By inspection of figure 3, we find that the bandgap and the band offsets are fully developed at a distance of only 7–9 Å from the substrate, in agreement with electron energy-loss spectroscopy data [2].

The determination of the band edges allows the identification of silicon-induced gap states (IGSs). Within the oxide, these are evanescent states with energies located in the bandgap, hence they can be singled out by inspecting the local density of states. The decay length of induced gap states in the oxide can be evaluated through a linear fit of the charge density in a logarithmic plot. In particular, focusing on the IGS near the Si band edges, we calculated a decay length in the oxide of $\simeq$1.2 Å for both hole and electron IGSs. This result is in good agreement with measurements of leakage current density as a function of oxide thickness, which give a current decay rate of about one decade per 2 Å of oxide thickness [51]. Indeed, on the basis of a simple model for the tunnelling current [52], this estimate can be translated into an IGS decay length of 1.15 Å, quite close to the value we found for the oxide in our model structures.

5. Dielectric properties

For the model interfaces considered in this work, we mapped both the high-frequency and the static permittivities across the interface. The permittivity profile was obtained by determining the microscopic response to a finite electric field applied from the outside [53, 54]. The local permittivity provides a good approximation to the full nonlocal permittivity tensor when length scales of the order of interatomic distances are considered [55]. For this purpose, we smoothed all the microscopic quantities through a Gaussian filter with a standard deviation of 1 Å. Here we consider a reference frame with the x-axis perpendicular to the Si–SiO_2 interface plane. Through the induced microscopic polarization $p_x(x)$ and the selfconsistent microscopic electric field $e_x(x)$ which arise upon the onset of the external field, we calculated the local permittivity $\varepsilon_{xx}(x)$ according to $\varepsilon_{xx}(x) = 1 + 4\pi p_x(x)/e_x(x)$. In the remainder of this section we will use $\varepsilon(x)$ as a shorthand notation for $\varepsilon_{xx}(x)$. In particular, we will consider two situations of practical relevance, namely the static permittivity $\varepsilon^0(x)$ and the high-frequency permittivity $\varepsilon^\infty(x)$.

Figure 4 shows the calculated profiles of the high-frequency and the static permittivity across our interface models, in the superlattice geometry described in section 2. The salient

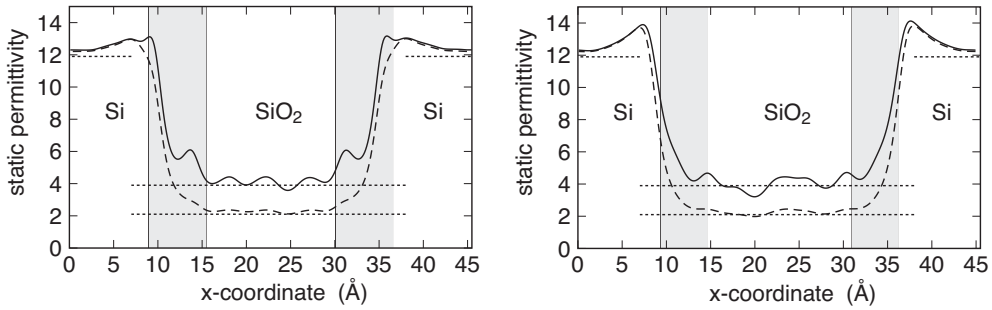

Figure 4. Dielectric permittivity profiles of model I (left) and model II (right) of the Si(100)–SiO_2 interface. Solid lines indicate the static permittivity, dashed lines the high-frequency permittivity. The x-coordinate is taken along a direction perpendicular to the interface plane. Horizontal dotted lines correspond to the experimental values. The shaded areas indicate the suboxide regions.

Table 3. Calculated high-frequency and static permittivities of the silicon, suboxide and oxide regions for models I and II of the Si(100)–SiO_2 interface.

	$\varepsilon^{\infty}_{\mathrm{Si}}$	$\varepsilon^{0}_{\mathrm{Si}}$	$\varepsilon^{\infty}_{\mathrm{SiO}_x}$	$\varepsilon^{0}_{\mathrm{SiO}_x}$	$\varepsilon^{\infty}_{\mathrm{SiO}_2}$	$\varepsilon^{0}_{\mathrm{SiO}_2}$
Model I	12.4	12.5	4.2	6.9	2.3	4.2
Model II	12.3	12.5	3.4	5.7	2.3	4.0
Experiment	11.9	11.9	—	6–7[a]	2.1	3.9

[a] Reference [21].

features are also reported in table 3. The high-frequency and static permittivities in the middle of the Si slab approximately coincide, due to the vanishing dynamical charges at a sufficiently large distance from the interface. The calculated static permittivity, $\varepsilon^{0}_{\mathrm{Si}} = 12.5$ for both model interfaces, slightly overestimates the experimental value of 11.9, mainly because of the inherent error of the adopted density functional scheme [56]. We evaluated an average high-frequency permittivity of 2.3 for the stoichiometric oxides of both model interfaces. The corresponding static permittivities are 4.2 and 4.0 for model I and model II, respectively. Also in this case, the calculated permittivities slightly overestimate the experimental values (2.1 and 3.9 for the high-frequency and the static permittivity, respectively). The difference between the static permittivities of the oxides in our models can be traced back to their different mass densities. The permittivities of the substoichiometric oxide amount to $\varepsilon_{\mathrm{SiO}_x} = 6.9$ and $\varepsilon_{\mathrm{SiO}_x} = 5.7$ for model I and model II, respectively. The difference mainly arises from the different spatial distributions and orientations of the suboxide Si–Si bonds. Our calculations are consistent with indirect experimental measurements which assign a static permittivity between 6 and 7 to the interfacial layer [21]. Furthermore, figure 4 shows that the permittivity of bulk SiO_2 is recovered as soon as the Si atoms become fully oxidized, i.e. at a distance of about 5–6 Å from the substrate. This result is consistent with Auger measurements indicating that the bulk SiO_2 high-frequency permittivity is already recovered at a distance of 6 Å from the substrate. Finally, a detailed analysis shows that the enhanced permittivity in the outermost Si layers of the substrate results from the screening provided by Si–Si bonds in the adjacent suboxide [55].

The enhanced permittivity of the suboxide region has previously been related to the silicon-induced gap states discussed in section 4 [2, 57]. In order to investigate the role of such states, we evaluated their contribution to the screening of the interfacial oxide through an approach based on maximally localized Wannier functions [53]. The IGS contribution to the dielectric screening in the interfacial layer was found to be only a small fraction (13%) of the

high-frequency permittivity in that region, indicating that their role is indeed secondary. At variance, we found that the permittivity enhancement is chemical in origin, being related to the larger polarizability of the structural units associated with partially oxidized Si atoms.

The enhanced permittivity of the interfacial oxide has clearly important technological implications in the area of high-permittivity dielectrics [58]. In addition, our results bear some consequences in the area of thin-film metrology. Indeed, when the permittivity enhancement near the substrate is neglected, standard techniques for the determination of film thickness such as spectroscopic ellipsometry and capacitance–voltage can yield measured thicknesses differing by 0.2–0.3 nm from the corresponding physical thicknesses [59].

6. Conclusion

We reviewed the structural, electronic and dielectric properties of two atomistic models of the Si(100)–SiO_2 interface. These models were specifically designed in order to match a large variety of available experimental data. After generating, refining and selecting only those models which fulfil a number of constraints set by experimental data, we studied their electronic structures and mapped the local dielectric permittivity across the interfacial layer. The good agreement of the calculated electronic and dielectric properties with experiment indicates once more that these models indeed give a realistic description of the actual interface between silicon and its oxide.

Acknowledgments

The calculations were performed at the computational facilities of the DIT-EPFL and the CSCS.

References

[1] Schulz M 1999 *Nature* **399** 729
[2] Muller D A, Sorsch T, Moccio S, Baumann F H, Evans-Lutterodt K and Timp G 1999 *Nature* **399** 758
[3] Wilk G D, Wallace R M and Anthony J M 2001 *J. Appl. Phys.* **89** 5243
[4] Van Elshocht S, Caymax M, De Gendt S, Conard T, Pétry J, Daté L, Pique D and Heyns M M 2004 *J. Electrochem. Soc.* **151** F77
[5] Diebold A C, Venables D, Chabal Y, Muller D, Weldon M and Garfunkel E 1999 *Mater. Sci. Semicond. Proc.* **2** 103
[6] Awaji N, Ohkubo S, Nakanishi T, Sugita Y, Takasaki K and Komiya S 1996 *Japan. J. Appl. Phys.* **35** L67
[7] Kosowsky S D, Pershan P S, Krish K S, Bevk J, Green M L, Brasen D and Feldman L C 1997 *Appl. Phys. Lett.* **70** 3119
[8] Witczak S C, Suehle J S and Gaitan M 1992 *Solid-State Electron.* **35** 345
[9] Stesmans A and Afanas'ev V V 1998 *J. Phys.: Condens. Matter* **10** L19
[10] Himpsel F J, McFeely F R, Taleb-Ibrahimi A, Yarmoff J A and Hollinger G 1988 *Phys. Rev.* B **38** 6084
[11] Lu Z H, Graham M J, Jiang D T and Tan K H 1993 *Appl. Phys. Lett.* **63** 2941
[12] Rochet F, Poncey C, Dufour G, Roulet H, Guillot C and Sirotti F 1997 *J. Non-Cryst. Solids* **216** 148
[13] Oh J H, Yeom H W, Hagimoto Y, Ono K, Oshima M, Hirashita N, Nywa M and Toriumi A 2001 *Phys. Rev.* B **63** 205310
[14] Pasquarello A, Hybertsen M and Car R 1995 *Phys. Rev. Lett.* **64** 1024
[15] Pasquarello A, Hybertsen M and Car R 1996 *Phys. Rev.* B **53** 10942
[16] Pasquarello A, Hybertsen M and Car R 1996 *Appl. Phys. Lett.* **68** 625
[17] Pasquarello A, Hybertsen M and Car R 1996 *Appl. Surf. Sci.* **104/105** 317
[18] Pasquarello A and Hybertsen M 2000 *The Physics and Chemistry of SiO_2 and the Si–SiO_2 Interface* ed H Z Massoud, I Baumvol, M Hirose and E H Poindexter (Pennington: Electrochemical Society) p 271
[19] Bongiorno A and Pasquarello A 2002 *Mater. Sci. Eng.* B **96** 102
[20] Hirose K, Kitahara H and Hattori T 2003 *Phys. Rev.* B **67** 195313

[21] Perkins C M, Triplett B B, Mclntyre P C, Saraswat K C, Haukka S and Tuominen M 2001 *Appl. Phys. Lett.* **78** 2357
[22] Pasquarello A, Hybertsen M and Car R 1998 *Nature* **396** 58
[23] Pasquarello A, Hybertsen M and Car R 2001 *Fundamental Aspects of Silicon Oxidation* ed Y J Chabal (Berlin: Springer) p 107
[24] Buczko R, Pennycook S J and Pantelides S T 2000 *Phys. Rev. Lett.* **84** 943
[25] Tu Y and Tersoff J 2000 *Phys. Rev. Lett.* **84** 4393
[26] Yamasaki T, Kaneta C, Uchiyama T, Uda T and Terakura K 2001 *Phys. Rev.* B **63** 115314
[27] Hane M, Miyamoto Y and Oshiyama A 1990 *Phys. Rev.* B **41** 12637
[28] Ng K O and Vanderbilt D 1999 *Phys. Rev.* B **59** 10132
[29] Watanabe T, Fujiwara H, Noguchi H, Hoshino T and Ohdomari I 1999 *Japan. J. Appl. Phys.* **38** L366
[30] Watanabe T and Ohdomari I 1999 *Thin Solid Films* **343/344** 370
[31] Bongiorno A and Pasquarello A 2003 *Appl. Phys. Lett.* **83** 1417
[32] van Beest B W H, Kramer G J and van Santen R A 1990 *Phys. Rev. Lett.* **64** 1955
[33] Bongiorno A, Pasquarello A, Hybertsen M S and Feldman L C 2003 *Phys. Rev. Lett.* **90** 186101
[34] Stensgaard I, Feldman L C and Silverman P J 1978 *Surf. Sci.* **77** 513
[35] Bongiorno A, Pasquarello A, Hybertsen M S and Feldman L C 2004 *Microelectron. Eng.* **72** 197
[36] Dal Corso A, Pasquarello A, Baldereschi A and Car R 1996 *Phys. Rev.* B **53** 1180
[37] Vanderbilt D 1990 *Phys. Rev.* B **41** 7892
[38] Perdew J P and Wang J 1992 *Phys. Rev.* B **46** 12947
[39] Pasquarello A, Laasonen K, Car R, Lee C and Vanderbilt D 1992 *Phys. Rev. Lett.* **69** 1982
[40] Laasonen K, Pasquarello A, Car R, Lee C and Vanderbilt D 1993 *Phys. Rev.* B **47** 10142
[41] Car R and Parrinello M 1985 *Phys. Rev. Lett.* **55** 2471
[42] Bongiorno A and Pasquarello A 2000 *Phys. Rev.* B **62** R16326
[43] Mauri F, Pasquarello A, Pfrommer B G, Yoon Y G and Louie S 2000 *Phys. Rev.* B **62** R4786
[44] Nakajima K, Joumori S, Suzuki M, Kimura K, Osipowicz T, Tok K L, Zheng J Z, See A and Zhang B C 2003 *Appl. Phys. Lett.* **83** 296
[45] Bongiorno A and Pasquarello A 2004 *Appl. Surf. Sci.* **234** 190
[46] Colombo L, Resta R and Baroni S 1991 *Phys. Rev.* B **44** 5572
[47] Keister J W, Rowe J E, Kolodziej J J, Niimi H, Madey T E and Lucovsky G 1999 *J. Vac. Sci. Technol.* B **17** 1831
[48] Afanas'ev V V, Houssa M, Stesmans A and Heyns M M 2001 *Appl. Phys. Lett.* **78** 3073
[49] Tuttle B R 2003 *Phys. Rev.* B **67** 155324
[50] Watarai M, Nakamura J and Natori A 2004 *Phys. Rev.* B **69** 035312
[51] Green M L, Sorsch T W, Timp G L, Muller D A, Weir B E, Silverman P J, Moccio S V and Kim Y O 1999 *Microelectron. Eng.* **48** 25
[52] Tomfohr J K and Sankey O F 2002 *Phys. Status Solidi* b **233** 59
[53] Giustino F, Umari P and Pasquarello A 2003 *Phys. Rev. Lett.* **91** 267601
[54] Umari P and Pasquarello A 2002 *Phys. Rev. Lett.* **89** 157602
[55] Giustino F and Pasquarello A 2005 *Phys. Rev.* B at press
[56] Gonze X, Ghosez P and Godby R W 1995 *Phys. Rev. Lett.* **74** 4035
[57] Muller D A and Wilk G D 2001 *Appl. Phys. Lett.* **79** 4195
[58] Copel M, Reuter M C and Jamison P 2004 *Appl. Phys. Lett.* **85** 458
[59] Chang H S, Yang H D, Hwang H, Cho H M, Lee H J and Moon D W 2002 *J. Vac. Sci. Technol.* B **20** 1836